Better than 10 mA Field Emission from an Isolated Structure Emitter of a Metal Oxide/CNT Composite

Wal Jun Kim,[†,‡] Jeong Seok Lee,[†,‡] Seung Min Lee,[†,‡] Ki Young Song,[†] Chong Nam Chu,[†] and Yong Hyup Kim[†,‡,*]

[†]School of Mechanical and Aerospace Engineering and [‡]Institute of Advanced Aerospace Technology, Seoul National University, San 56-1, Sillim-dong, Kwanak-gu, Seoul 151-742, Korea

ABSTRACT An isolated structure emitter is presented that can deliver a field emission better than 10 mA, a level that is by far the highest ever reported. A composite of CNT (carbon nanotube) and WO_3 is used to grow the point emitter by a crystal-like growth technique. The head of the grown needle that is the emitter is removed by electric discharge machining (EDM). The EDM treatment not only controls the length of the emitter as desired but also makes the tip of the emitter uniform. The thermal heat due to EDM treatment leads to the formation of a tungsten carbide phase, which results in a 3 orders of magnitude reduction in contact resistance. The point emitter is robust in its stability, as evidenced by its on-time resilience against a severe bias test.

KEYWORDS: field emission · emitter · metal oxide/CNT composite · electric discharge machining · crystal-like growth technique

Field emission from an individual carbon nanotube (CNT)[1] and a thin film CNT[2] discovered in the mid-90s has spurred development of CNT emitters for applications in field emission display,[3−5] X-ray sources,[6,7] microwave amplifier,[8,9] and high-resolution electron beam instruments.[10] Planar CNT emitters fabricated by screen printing and chemical vapor deposition have drawn interest for practical application in field emission display.[9,11−13] Point emitters, in general, are preferred for applications in X-ray sources and electron beam instruments because of a small spot size for electron emission[14,15] and field emission properties better than those of planar emitters due to the high aspect ratio of the point emitter. It is, however, more difficult to fabricate a well-defined structure of the point emitters than the planar ones.

Two types of fabrication techniques are usually used for the point emitter, direct and indirect. In the direct method, CNTs are grown at the point where a catalyst is placed by chemical vapor deposition.[16,17] The direct method requires selective deposition of catalyst and high temperature heating for growing the CNTs. In this method, it is difficult to control the length and vertical alignment of grown CNTs. The indirect methods involve transfer of preformed CNTs onto a sharpened or pointed substrate. These include glue method,[10] dielectrophoresis,[18−20] and spinning technique.[21−23] In the glue method, as-grown CNTs can be manually attached to the substrate that is coated with adhesive material by trial and error. Dielectrophoresis utilizes the interaction between external electric field and the induced dipole moment of CNTs suspended in a solution. However, it is difficult to attach a single CNT or a few CNTs that are vertically aligned on a substrate. The macroscopic CNT point emitter fabricated by the spinning technique utilizes multiwalled carbon nanotube (MWNT) yarn. This method also requires an adhesive and manual manipulation. Both direct and indirect methods lead to a CNT point emitter that is poor in electrical contact and weak in the mechanical strength between substrate and CNT structure. These problems result in a poor emitter performance and poor emitter stability with time.

In this work, we present an isolated structure emitter made of a WO_3/CNT composite that produces a current larger than 10 mA, which exceeds the highest level ever reported (3 mA) by a wide margin, and yet maintains its robustness in terms of long-term stability.[23] The fabrication involves two distinct steps of growing a macroscopic CNT composite emitter followed by electrical discharge machining (EDM) treatment of the grown emitter. For the growth, a crystal-like growth technique[24] is utilized. The EDM treatment is used to control the emitter length and endow the treated emitter with highly desirable properties for the field emission.

*Address correspondence to yongkim@snu.ac.kr.

Received for review August 9, 2010 and accepted December 10, 2010.

Published online December 20, 2010. 10.1021/nn101956w

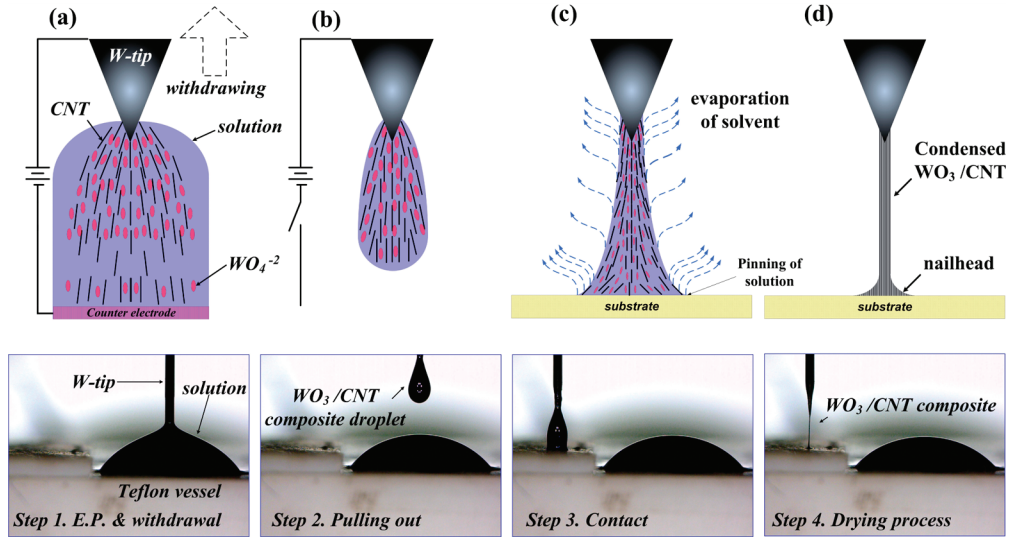

Figure 1. Schematic of the procedure for fabricating a one-dimensional WO_3/CNT composite structure by crystal-like growth: (a) immersing tungsten tip into stable CNT suspension and electrolyte in DMF and beginning electroplating with bias applied between W tip and counter electrode, (b) pulling up the WO_3/CNT composite from the solution at a faster rate to finish the growth, (c) contacting the WO_3/CNT composite on Teflon substrate to avoid curling effect. (d) Drying of solvent for the condensed WO_3/CNT composite, resulting in a vertically aligned composite emitter. The bottom row frames show the digital snapshots of each step of the procedure.

RESULTS AND DISCUSSION

Shown in Figure 1 is a schematic of the procedure involved in the fabrication of the WO_3/CNT composite with nonaqueous electrolyte (Experimental Section). The bottom frames show actual optical pictures of the fabrication steps. As shown in Figure 1a, a sharpened tungsten tip is immersed into the electrolyte solution, which is CNT and sodium tungstate dissolved in DMF solvent for the WO_3/CNT composite being fabricated. In the schematic, the red dots are WO_4^{2-} ions, and dark straight lines represent CNTs. Upon applying bias to the tungsten anode with the container bottom grounded, negatively charged CNTs that are acid-treated gather around the anode along with the WO_4^{2-} ions. After electroplating for 5 min with constant current of 1 mA, the electrode is pulled up at a speed of 0.3 mm/min with a column of the solution of CNTs and WO_4^{2-} clinging to the tungsten tip. The bias is still on during the pulling. After the desired length of the macroscopic one-dimensional WO_3/CNT composite is reached, the electrode is quickly pulled up to complete the electroplating, as shown in Figure 1b. The tip of the withdrawn WO_3/CNT column is carefully placed on a Teflon plate and is made to touch its surface. As shown in Figure 1d, the solvent in the exposed column of solution evaporates, leading eventually to the formation of a condensed macroscopic one-dimensional CNT structure having a diameter of about 20 μm. Without the contact process, the composite emitter eventually curls due to inhomogeneous evaporation of solvent from the surface of the column. Therefore, the contact that mechanically constrains the free end of the column is a key to vertically aligning the composite along the axis of the tungsten tip. Finally, the composite emitter is introduced into the furnace and then heated to 600 °C in nitrogen ambient atmosphere to remove residual solvent.

Figure 2b shows the macroscopic one-dimensional CNT composite emitter 2 mm long and 20 μm in diameter that was fabricated at a current level of 1 mA. The magnified scanning electron microscopy (SEM) image

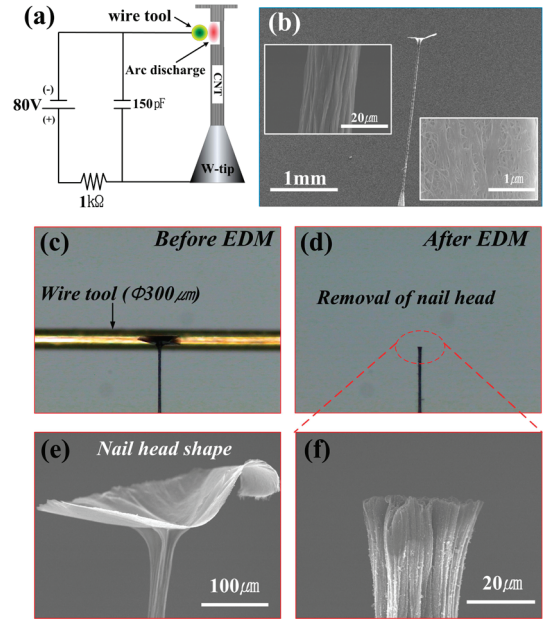

Figure 2. (a) Schematic of the EDM treatment. The applied voltage was 80 V (dc). (b) SEM (scanning electron microscopy) image of whole feature of the WO_3/CNT composite emitter. The insets show magnified SEM micrographs of well-aligned SWNT bundles along the axis of the composite emitter. (c) Optical image of the WO_3/CNT composite emitter with nail head shape and EDM wire tool with a diameter of 0.3 mm before EDM treatment. (d) Optical image of the emitter with the nail head removed by EDM treatment. (e,f) SEM images before and after EDM treatment, respectively.

of the structure in the inset of Figure 2b reveals the outside texture that appears to be cylindrical cords bound together in the direction of growth, which are somewhat interwoven. The alignment is a result of the surface tension of the solution exerted on the WO_3/CNT composite network that was generated by electroplating and by the upward movement of the electrode.

The shape of the tip that results after the drying resembles a nail head, as the magnified SEM image of Figure 2e shows. The nail head results from a pinning effect[25] that was generated by capillary flow in which the contact line of the drying column on the Teflon plate is replenished by solvent from the interior as the solvent evaporates from the edge. The resulting outflow of solvent carries dispersed WO_3/CNT nanomaterials to the edge. For a point emitter, the nail head shape at the tip of the composite emitter is not desirable because it is difficult to obtain reproducible field emission properties, and the thin nail head is vulnerable to degradation in high current field emission.

Electrical discharge machining (EDM) technique was used to remove the undesirable nail head. Electrical discharge can take place when a voltage is applied between a conductive tool electrode and a conductive material placed in a dielectric fluid. When the distance between the two conductors becomes small enough, the dielectric fluid breaks down, causing an electric discharge between them. The high frequency sparks create a very high temperature at localized spots on the electrodes. The material then melts and evaporates. Since EDM is basically a thermal machining process, any conductive material can be machined regardless of its mechanical strength.[26,27] A schematic of EDM treatment is shown in Figure 2a. The composite emitter, with a length of 2 mm and a diameter of 20 μm, was machined by a one directional moving wire tool that is 0.3 mm in diameter. The feed rate was set at 2 μm/s, which was slow enough to prevent a short between the composite emitter and the wire tool. The EDM treatment was conducted in air to prevent the composite emitter from being contaminated or damaged in a dielectric fluid, such as kerosene, which is generally used in the EDM process. The sequence of the nail head being removed is clearly shown in the images of EDM treatment shown in Figure 2c−f.

The EDM process, in general, can raise the temperature to a range of 8000−12 000 °C.[28] This high temperature spark can have a significant impact on the crystallinity of the composite emitter. For the examination, Raman spectroscopy based on a micro-Raman system (JY-Horiba, LabRam 300) was employed with 647 nm line of CW Kr ion laser (Coherent, Innova 300C) excitation source. The peak at 1583 cm^{-1} (G band) in the Raman spectrum is associated with the hexagonal lattice of graphite, while the peak at 1355 cm^{-1} (D band) indicates the level of carbon disorder. The intensity ratio of I_D to I_G is an indicator of CNT crystallinity. When the composite emitter (1 mm long) in Figure 3a was subjected to EDM, the intensity ratio of 0.07678, 0.07953, and 0.06489 corresponding to the column tip, middle, and bottom, respectively, increased to 0.808, 0.1927, and 0.5397 after the EDM treatment. These ratios indicate that the EDM process damaged the composite structure. The CNTs in the tip part of the emitter were subjected to a very high temperature and evaporated. As a result, the ratio increased dramatically. Similar conclusion could be drawn with regard to the crystallinity at the other positions of the middle and bottom of the emitter column. An interesting outcome of the treatment is that the ratio at the bottom became larger than that at the middle after the treatment.

The anomaly at the bottom position could be explained by the high current of 7 A that passed through the composite emitter during the arc discharge. The current-induced Joule heating that could cause the disordering must be much more extensive at the bottom than at the middle because of the presence of the interface between the tungsten tip and the composite, which apparently led to a large ratio at the bottom.

The total resistance of the emitter consists of three resistances in series: tungsten resistance, composite resistance, and the resistance at the W−composite interface. Its value as determined by a two-terminal probe station was 48 kΩ, while that of the composite was 6.58Ω ($\rho = 7.58 \times 10^{-4}$ Ωcm) before the EDM treatment. We were pleasantly surprised to find that the total resistance was reduced to 70 Ω from 48 kΩ after the EDM treatment, almost a 3 orders of magnitude reduction in the resistance. To probe reasons for the drastic reduction in the total resistance, individual resistances making up the total were measured. Tungsten resistance remained almost the same at around 1.2 Ω regardless of the treatment. The emitter resistance increased to 32 from 6.58 Ω due to the treatment, as given in Figure 3e. Since the two resistances together with the interfacial resistance make up the total resistance, the interfacial resistance before and after EDM treatment can be calculated to be 47.8 kΩ before and 36.5 Ω after the treatment.

A recent study[29,30] sheds light on a plausible cause for the tremendous reduction in the interfacial resistance. Because of a very high level of Joule heating caused by the arc discharge, tungsten could be in a liquid state and carbon in the CNT could diffuse into the molten tungsten, eventually forming a WC phase. It is well-known that tungsten carbide is a good conductor.[29] To confirm the carbide formation, X-ray photoluminescence spectroscopy (XPS) was carried out. The spectra before and after the treatment are shown in the top and bottom part of Figure 3f, respectively. The lower part reveals (C 1s) the peak, and its deconvolution clearly indicates the presence of C−W bonding. The binding energy at 283.5 eV agrees with that reported for tungsten carbide.[31,32]

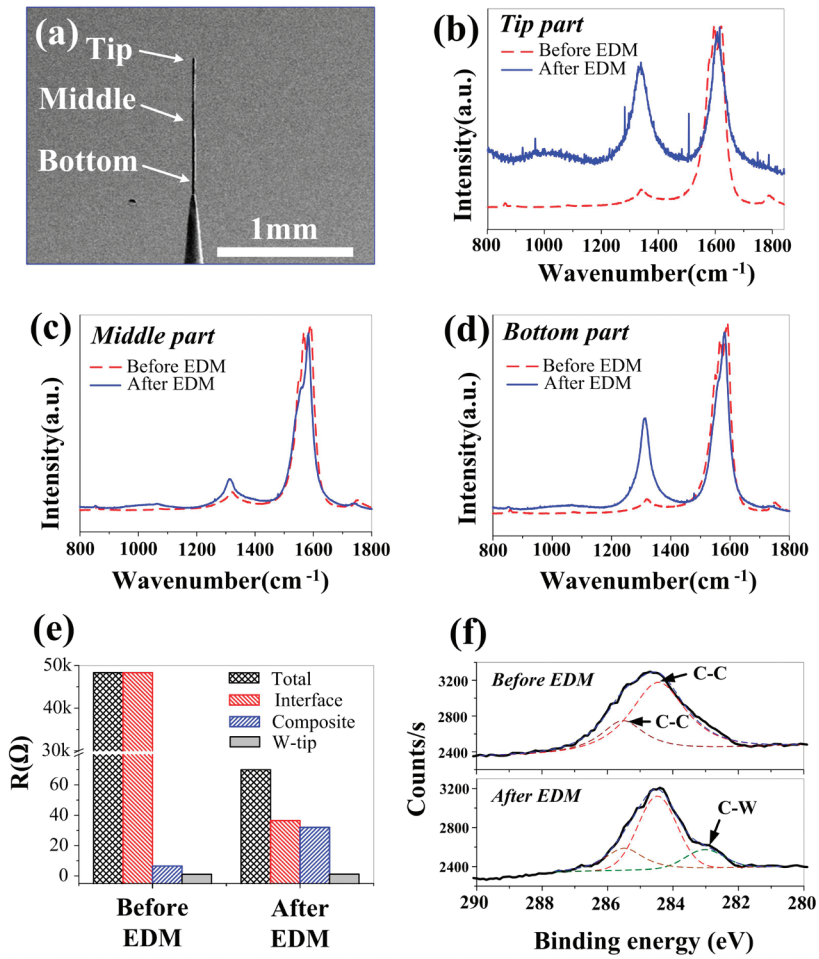

Figure 3. (a) WO_3/CNT composite emitter after removal of the nail head. (b,d) Raman spectrum based on the location of the composite emitter of two cases, before EDM and after EMD treatment. (e) Graph shows the change of the resistance of the composite, which consists of three resistance components: resistance of W tip, that of the composite and the contact or interface resistance between the W tip and the composite. (f) Deconvoluted carbon XPS spectra of the junction between CNT composite and W tip. Top and bottom graphs show the spectra before and after EDM treatment, respectively.

The field emission characteristics of these composite emitters were measured using point-plane configuration in a vacuum chamber at a base pressure of 2.0×10^{-7} Torr. As shown in Figure 4a, the field emission current of the EDM-treated composite emitter reached the maximum level of 10 mA that is allowed by our dc power equipment and a threshold field less than 0.6 V/μm. We believe that the lower threshold field can be attributed to a high aspect ratio of the EDM-treated composite emitter with a diameter of 20 μm and a length of 1 mm. This aspect ratio of the emitter is high enough to overcome the screen effect felt by individual

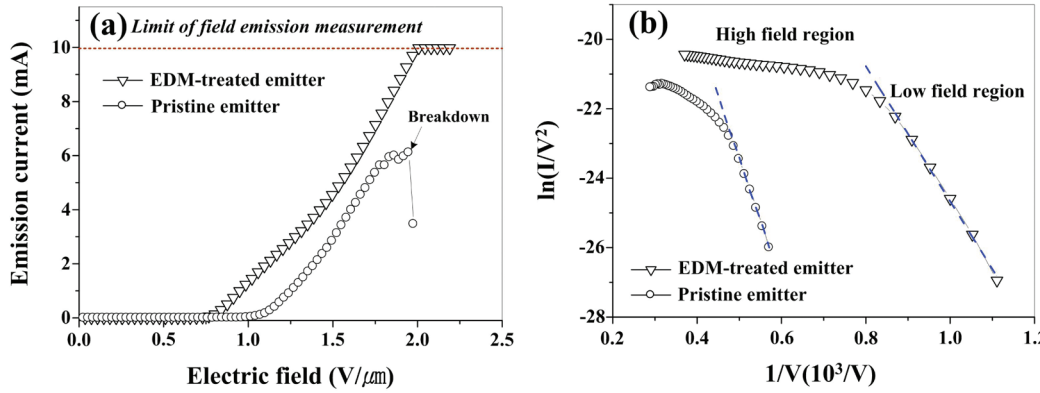

Figure 4. (a) *I*−*V* plots of pristine and EDM-treated emitters. (b) Fowler−Nordheim plots of field emission characteristics (*I*−*V* plot).

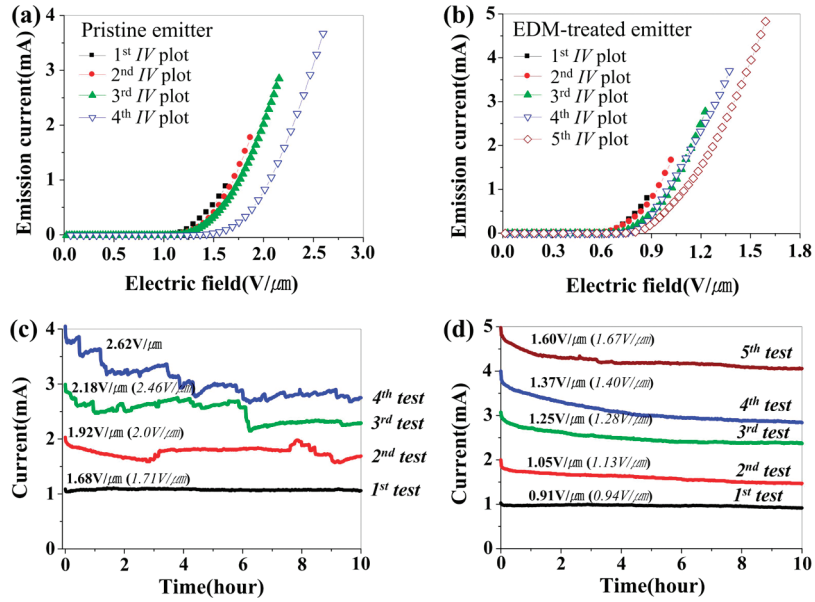

Figure 5. Field emission characteristics of composite emitters measured with point-plane configuration at base pressure of 2×10^{-7} Torr. (a,b) Current−voltage tests without and with EDM treatment; *n*th stability test was carried out between *n*th and (*n*+1)th current−voltage test. (c,d) Field emission stability of pristine and EDM-treated emitters, respectively. Boldface numbers and the numbers in the round bracket indicate applied electric field during stability test and the electric field which is required to obtain initial current level after the stability test.

nanotubes in the emitter. It has been shown,[13] for instance, that macroscopic turn-on electric field decreases as the length of CNTs is increased.

Judging from the robustness of the current−electric field curve at the maximum allowed 10 mA, which contrasts the typical behavior around the breakdown field as revealed by the same curve for the emitter without the treatment or pristine emitter at 6 mA, the emission current would have reached more than 10 mA had the dc equipment been one that could provide a current level higher than 10 mA. Even the current level reached by the pristine composite emitter before breakdown is higher than any reported in the literature.[18−23,33−35] The incredibly high current level of better than 10 mA of the EDM-treated emitter could be attributed to uniform geometric length of individual CNTs in the composite, large aspect ratio, high conductivity of the composite, and low contact resistance between W and the composite emitter.

Fowler−Nordheim plots are given in Figure 4b for both EDM-treated emitter and nontreated (pristine) emitter. The emission obeys the Fowler−Nordheim relationship in the low field region but deviates from the linearity in the high field region. A discussion on the nonlinearity can be found in Figure S1 (Supporting Information).

The stability of field emission is of practical interest at high current since the emitter can easily be damaged due to evaporation of CNTs by Joule heating and ion bombardment of residual gases. A severe stability test was conducted in which the emitter field was maintained constant at the level corresponding to 1 mA for 10 h, after which the level was increased to 2 mA for another 10 h. This procedure was repeated for 3 and 4 mA for the pristine emitter but one more step up to 5 mA for the EDM-treated emitter. Initially, and each time the current was increased by 1 mA, the current−electric field characteristics were also obtained and the results are given in Figure 5a,b for pristine and treated emitter, respectively. As shown in Figure 5c for pristine emitter, the current becomes jagged with time and the jaggedness gets worse as the current level is increased. For the EDM-treated emitter shown in Figure 5d, it is apparent that the current decreases monotonically with little fluctuation, showing its stability with on-time. The emission current density of 5 mA corresponds to approximately 1590 A cm^{-2} since the emitter diameter is about 20 μm, as shown in Figure 2b. As a result of EDM treatment, in general, the threshold field decreases and the field enhancement factor increases (see Figure S2 of Supporting Information). We believe that the excellent field emission properties of the WO_3/CNT emitter resulted from a lower contact resistance between the CNT emitter and tungsten tip substrate through the formation of tungsten carbide. We also believe that WO_3 played the role of an electron acceptor, resulting in a lower resistance of CNT emitter itself.[24] These factors contributed to the enhancement of field emission properties.

CONCLUSIONS

In summary, an isolated structure emitter has been presented for field emission that can deliver a current higher than 10 mA, which is by far the highest ever reported in the literature. The emitter has been shown to be robust and stable at high currents. The emitter

needle was grown by a crystal-like growth technique. The "nail head" that forms during the drying of the grown needle was removed by EDM. This cutting of the nail head leads to uniform geometric length of CNTs in the composite emitter, which contributed to the stability of the field emission. More importantly, the EDM treatment results in a dramatic decrease in the contact resistance between tungsten tip and the composite. This reduction has been found to be linked to the formation of tungsten carbide during the treatment that is a good conductor. As a result, we obtained the best of CNT point emitter in the world with high current and long-term stability. Therefore, we suggest that our WO_3/CNT composite emitter will be excellent candidate for high-performance X-ray source and electron beam instrument.

EXPERIMENTAL SECTION

Preparation of CNT Colloidal Solution Based on Nonaqueous Electrolyte and Sharpened Tungsten Tip. First of all, purified SWNT powder was prepared by filtering out wet acid treated CNTs (ASP-100F, Hanwha Nanotech Corp.), which were synthesized by arc discharge method. Then sodium tungstate ($Na_2WO_4 \cdot 2H_2O$, Aldrich) and the purified SWNT powder were mixed with 0.1 mg/mL, respectively. The solution was continuously sonicated for 10 h. CNT colloidal solution based nonaqueous electrolyte was filled in a Teflon vessel which has a diameter of 3 mm and a depth of 5 mm, and a counter electrode was placed on the bottom of the vessel. Meanwhile, a tungsten (The Nilaco Corporation, Japan) wire was electrochemically etched in KOH solution (1.5M) with an applied voltage of 30 V. Then we obtained a sharpened tungsten tip with the tip radius of curvature of 250 nm.

Electroplating System. The tungsten tip was immersed into the CNT colloidal solution in a container. The counter lectrode was placed in the bottom of the container. We carried out electroplating with Keithley 6220 Precision Current Source, which provided the tungsten tip and the counter electrode with a constant current ranging from 2 nA to 100 mA.

Electric Discharge Machining. Kerosene and deionized water are generally used as working fluids in the EDM process. The working fluid must be continuously replenished at the machining gap between the electrode and the workpiece. In this study, however, EDM process was performed in the air without replenishing to avoid the damage and contamination of the composite emitter. The $X-Y$ stage of the machining moves a workpiece and an electrode tool runs on the Z-axis with 0.1 μm resolution. The electrode was used by brass with a diameter of 300 μm.

X-ray Photoluminescence Spectroscopy. XPS spectra of tungsten oxide were measured using Sigma Probe (Thermo VG, U. K.) with Al Kα radiation. The binding energies of C 1s peaks were measured from 280 to 290 eV with a step of 0.1 eV, and the duration of one channel was 0.1 s.

Raman Spectroscopy. Micro-Raman system (JY-Horiba, LabRam 300) used a collimated 50× objective lens (Olympus, NA 0.75). This system is equipped with a thermoelectrically cooled charge-coupled device (CCD) detector, and the signal was obtained by 180° backscattering geometry. The 647 nm line of CW Kr ion laser (Coherent, Innova 300C) was used as a Raman excitation source.

Acknowledgment. This research was supported by Basic Science Research Program through the National Research Foundation of Korea (NRF) funded by the Ministry of Education, Science and Technology (No. 2009-0083512), the National Research Foundation of Korea (NRF) grant funded by the Korea government (MEST) (No. 2010-0000786), Basic Science Research Program through the National Research Foundation of Korea (NRF) funded by the Ministry Education, Science and Technology (No. 2010-0018736), funded by the Pioneer Research Center Program through the National Research Foundation of Korea funded by the Ministry of Education, Science and Technology (Grant No. 2010-0002217), and the second stage of the Brain Korea 21 Project in 2010.

Supporting Information Available: Detailed discussion about the Fowler−Nordheim plot in high electric field region of Figure 4b and threshold field and field enhancement factor from Figure 5a,b. This material is available free of charge *via* the Internet at http://pubs.acs.org.

REFERENCES AND NOTES

1. Rinzler, A. G.; Hafner, J. H.; Nikolaev, P.; Nordlander, P.; Colbert, D. T.; Smally, R. E.; Lou, L.; Kim, S. G.; Tomanek, D. *Science* **1995**, *269*, 1550–1553.
2. Heer, W. A.; Chatelain, A.; Ugarte, D. *Science* **1995**, *270*, 1179–1180.
3. Saito, Y.; Uemura, S.; Hamaguchi, K. *Jpn. J. Appl. Phys. Part 2* **1998**, *37*, 346–348.
4. Lee, N. S.; Chung, D. S.; Han, I. T.; Kang, J. H.; Choi, Y. S.; Kim, H. Y.; Park, S. H.; Jin, Y. W.; Yi, W. K.; Yun, M. J.; Jung, J. E.; Lee, C. J.; You, J. H.; Jo, S. H.; Lee, C. G.; Kim, J. M. *Diamond Relat. Mater.* **2001**, *10*, 265.
5. Choi, W. B.; Chung, D. S.; Kang, J. H.; Kim, H. Y.; Jin, Y. W.; Han, I. T.; Lee, Y. H.; Jung, Y. H.; Lee, N. S.; Park, G. S.; Kim, J. M. *Appl. Phys. Lett.* **1999**, 3129–3131.
6. Zang, J.; Yang, G.; Cheng, Y.; Gao, B.; Qiu, Q.; Lee, Y. Z.; Lu, J. P.; Zhou, O. *Appl. Phys. Lett.* **2005**, *86*, 184104.
7. Liu, Z.; Yang, G.; Lee, Y. Z.; Bordelon, D.; Lu, J.; Zhou, O. *Appl. Phys. Lett.* **2006**, *89*, 103111.
8. Suzuki, Y.; Kozeki, T.; Ono, S.; Murakami, H.; Ohtake, H.; Sarukura, N.; Nakajyo, T.; Sakai, F.; Aoki, Y. *Appl. Phys. Lett.* **2002**, *80*, 3280–3282.
9. Milne, W. I.; Tao, K. B. K.; Minoux, E.; Groening, O.; Gangloff, L.; Hudanski, L.; Schnell, J. P.; Dieumegard, D.; Peauger, F.; Bu, I. Y. Y.; Bell, M. S.; Legagneux, P.; Hasko, G.; Amaratunga, G. A. J. *J. Vac. Sci. Technol., B* **2006**, *24*, 345–348.
10. Jonge, N.; Lamy, Y.; Schoots, K.; Oosterkamp, T. H. *Nature* **2002**, *420*, 393–395.
11. Zhu, W.; Bower, C.; Zhou, O.; Kochanski, G.; Jin, S. *Appl. Phys. Lett.* **1999**, *75*, 873–875.
12. Calderon-Colon, X.; Geng, H.; Gao, B.; An, L.; Cao, G.; Zhou, O. *Nanotechnology* **2009**, *20*, 325707.
13. Jo, S. H.; Tu, Y.; Huang, Z. P.; Carnahan, D. L.; Wang, D. Z.; Ren, Z. F. *Appl. Phys. Lett.* **2003**, *82*, 3520–3522.
14. Fursey, G. N. *Appl. Surf. Sci.* **2003**, *215*, 113–134.
15. Jonge, N. *J. Appl. Phys.* **2004**, *95*, 673–681.
16. Hafner, J. H.; Cheung, C. L.; Lieber, C. M. *Nature* **1999**, *398*, 761–762.
17. Cheung, C. L.; Hafner, J. H.; Odom, T. W.; Kim, K.; Lieber, C. M. *Appl. Phys. Lett.* **2000**, *76*, 3136–3138.
18. Zhang, J.; Tang, J.; Yang, G.; Qiu, Q.; Qin, L. C.; Zhou, O. *Adv. Mater.* **2004**, *14*, 1219–1221.
19. Jung, S. I.; Choi, J. S.; Shim, H. C.; Kim, S.; Jo, S. H.; Lee, C. J. *Appl. Phys. Lett.* **2006**, *89*, 233108.
20. Lim, S. C.; Lee, D. S.; Choi, H. K.; Lee, I. H.; Lee, Y. H. *Diamond Relat. Mater.* **2009**, *18*, 1435–1439.
21. Zakhidov, A. A.; Nanjundaswamy, R.; Obraztsov, A. N.; Zhang, M.; Fang, S.; Klesch, V. I.; Baughman, R. H.; Zakhidov, A. A. *Appl. Phys. A: Mater. Sci. Process.* **2007**, *88*, 593–600.
22. Wei, Y.; Jiang, K.; Liu, L.; Chen, Z.; Fan, S. *Nano Lett.* **2007**, *7*, 3792–3797.
23. Chen, G.; Shin, D. H.; Roth, S.; Lee, C. J. *Nanotechnology* **2009**, *20*, 3135201.
24. Kim, W. J.; Jang, E. Y.; Seo, D. K.; Kang, T. J.; Jin, K. C.; Jeong, D. H.; Jim, Y. H. *Langmuir* **2010**, *26*, 15701–15705.

25. Deegan, R. D.; Bakajin, O.; Dupont, T. F.; Huber, G.; Nagel, S. R.; Witten, T. A. *Nature* **1999**, *389*, 827–829.
26. Allenn, D. M. In *Micromachining of Engineering Materials*; McGeough, Dekker: New York, 2002.
27. Shobert, E. I. In *Electrical Discharge Machining: Tooling, Methods, and Applications*; Jameson, E. C., Ed.; Society of Manufacturing Engineers: Dearborn, MI, 1983; pp 3−4.
28. Boothroyd, G. Winston, A. K. *Fundamentals of Machining and Machine Tools*; Dekker: New York, 1989; p 491.
29. Wang, M. S.; Golberg, D.; Bando, Y. *Adv. Mater.* **2010**, *22*, 93–98.
30. Zhang, Y.; Ichihashi, T.; Landree, E.; Nihey, F.; Iijima, S. *Science* **1999**, *285*, 1719–1721.
31. Monteiro, O. R.; Delplancke-Ogletree, M. P.; Lo, R. Y.; Winand, R.; Brown, I. *Surf. Coat. Technol.* **1997**, *94−95*, 220–225.
32. Rincon, C.; Zambrano, G.; Carvajal, A.; Prieto, P.; Galindo, H.; Martinez, E.; Lousa, A.; Esteve, J. *Surf. Coat. Technol.* **2001**, *148*, 277–283.
33. Smith, R. C.; Cox, D. C.; Silva, S. R. P. *Appl. Phys. Lett.* **2005**, *87*, 103112.
34. Wei, Y.; Weng, D.; Yang, Y.; Zhang, X.; Jang, K.; Liu, L.; Fan, S. *Appl. Phys. Lett.* **2006**, *89*, 063101.
35. Sim, H. S.; Lau, S. P.; Ang, L. K.; You, G. F.; Tanemura, M.; Yamaguchi, K.; Zamri, M.; Yusop, M. *Appl. Phys. Lett.* **2008**, *93*, 023131.